From Formulation to Structure: 3D Electron Diffraction for Structure Solution of a New Indomethacin Polymorph from an Amorphous Solid Dispersion

Authors

Helen W. Leung[a]*, Royston C. B. Copley[b], Giulio I. Lampronti[a], Sarah J. Day[c], Lucy K. Saunders[c], Duncan N. Johnstone[b], Paul A. Midgley[a]*

[a] Department of Materials Science and Metallurgy, University of Cambridge, 27 Charles Babbage Road, Cambridge, CB3 0FS, United Kingdom
E-mail: pam33@cam.ac.uk
[b] GSK Medicines Research Center
Gunnels Wood Road, Stevenage, SG1 2NY, United Kingdom
[c] Diamond Light Source Ltd, Beamline I11
Harwell, Oxford, OX11 0DE, United Kingdom

Synopsis 3D electron diffraction (3D-ED) was used to elucidate the structure of a new ninth polymorph of indomethacin from an amorphous solid dispersion (ASD), which are product formulations used to improve dissolution performance of active pharmaceutical ingredients (APIs) with poor aqueous solubility. Insights from the structure solution allowed for a simpler synthesis route for this polymorph to be deduced, demonstrating the relevance of 3D-ED within drug development.

Abstract 3D electron diffraction is being used increasingly to determine molecular and crystal structures from micro-crystals. Indomethacin is a well-known marketed small molecule non-steroidal anti-inflammatory drug with eight known polymorphic forms, of which four have had their structures elucidated to date. Using 3D electron diffraction, we determine the structure of a new ninth polymorph σ found within an amorphous solid dispersion, a product formulation sometimes used for active pharmaceutical ingredients with poor aqueous solubility. Subsequently, we find that σ indomethacin can be produced from direct solvent evaporation using dichloromethane. These results demonstrate the relevance of 3D electron diffraction within drug development to directly probe product formulations.

Keywords: Indomethacin; amorphous solid dispersion; drug development; 3D electron diffraction; polymorphism; structure determination; pharmaceutical formulation

1. Introduction

Interest in 3D electron diffraction (3D-ED) techniques for structure solution from micro-crystals has increased rapidly within drug discovery over the past 5 years (Gemmi *et al.*, 2019; Jones *et al.*, 2018). 3D-ED (also known as MicroED) enables the determination of molecular structures from micro-crystals, eliminating the need for the larger crystals required for single-crystal X-ray diffraction (SCXRD), the current gold standard for structure solution in the pharmaceutical industry, and unlocks possibilities for high-throughput structure determination. The potential impact of 3D-ED within drug

development has been less prominent (Lightowler *et al.*, 2024): the majority of compounds with previously unknown structures which have been solved were of a single phase being studied in isolation, although there has also been success with determining structures from off-the-shelf products (Jones *et al.*, 2018; Karothu *et al.*, 2023; Gruene *et al.*, 2018). We present here a 3D-ED study on a type of sample that may be investigated at the product formulation stage of development, with the added complications of an unexpected form of the active pharmaceutical ingredient (API) and the presence of an excipient.

Indomethacin (Figure 1) is a non-steroidal anti-inflammatory drug known to have eight polymorphic forms (Table 1). Despite having been widely used for over 40 years, the structures of several polymorphs (δ and θ) have recently been revealed using 3D-ED (Lightowler *et al.*, 2022; Andrusenko *et al.*, 2021) . Indomethacin is classified using the Biopharmaceutics Classification System (BCS) as class II (Butler & Dressman, 2010), indicating its poor aqueous solubility and resulting in low oral bioavailability. Amorphous solid dispersions (ASDs) are a popular formulation strategy used to create superior dissolution performance, often referred to as the 'spring effect', of poorly soluble pharmaceutical molecules by creating a stable solid dispersion of the API within an amorphous water-soluble polymer, which acts as an excipient (Vasconcelos *et al.*, 2007). Furthermore, ASDs aim to provide kinetic stability to prevent subsequent crystallisation of the supersaturated drug within the gastrointestinal tract, often referred to as the 'parachute effect' (Hu *et al.*, 2019; Guzmán *et al.*, 2007). However, ASDs may experience storage life complications caused by unwanted phase separation and crystallisation of the API which may affect the performance of the drug product, subject to different storage conditions such as humidity and temperature (Ricarte *et al.*, 2019; Xie & Taylor, 2017). Undesirable crystallinity found in ASDs may take the form of different polymorphs (S'ari *et al.*, 2021). These can be difficult to isolate from the formulation in the form of a single crystal of sufficient quality for SCXRD. This may be further exacerbated by the presence of multiple polymorphs, resulting in potential concern late-on in the drug development process where the appearance of new forms can have serious consequences (Newman & Wenslow, 2016).

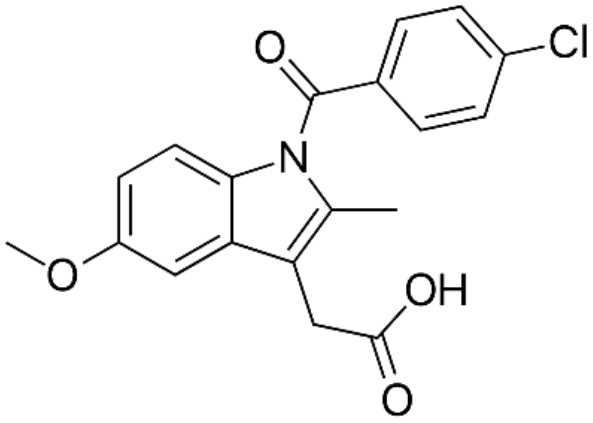

Figure 1 The indomethacin molecule $C_{19}H_{16}ClNO_4$.

Polymorph	Year Discovered	Year Solved	CSD Identifier	Method
γ	1968	1972 (Kistenmacher & Marsh, 1972)	INDMET (01, 03, 05, 06)	SCXRD
α	1968	2002 (Chen *et al.*, 2002)	INDMET02, 04	SCXRD
δ	1998	2021 (Andrusenko *et al.*, 2021; Lightowler *et al.*, 2022)	INDMET07, 08	3D-ED
ε	2013 (Surwase *et al.*, 2013)	-	-	-
η	2013 (Surwase *et al.*, 2013)	-	-	-
ζ	2013 (Surwase *et al.*, 2013)	-	-	-
τ	2018 (Van Duong *et al.*, 2018)	-	-	-
θ	2022	2022 (Lightowler *et al.*, 2022)	INDMET09	3D-ED

Table 1 A summary of the known polymorphic forms of indomethacin to date.

In this work, we formulate an ASD of indomethacin and polyvinylpyrrolidone (PVP), prepared via the solvent evaporation method using dichloromethane (Ricarte *et al.*, 2019). We find crystallinity in the form of a new polymorph of indomethacin which grows in a whisker-like (~30 nm wide) or lath-like (~ several hundred nm wide) morphology (see Figure 2a). We solve the structure of this new polymorph with 3D-ED.

2. Methods

The presence of a new crystal form in the ASD was first identified using X-Ray Powder Diffraction (XRPD). As expected, indomethacin purchased from Sigma Aldrich was as polymorph γ, the most stable form. Given that a range of drug loadings are commonly found in commercial ASDs, (He & Ho, 2015), ASDs across a range of drug loadings were produced using the solvent evaporation

method (S1.1). ASDs with loadings of 20:80 to 80:20 indomethacin/PVP appeared amorphous using XRPD. However, XRPD from 95:5 indomethacin/PVP ASDs feature a set of low angle characteristic peaks which could not be matched to any of the polymorphs of indomethacin in the Cambridge Structural Database (CSD) but instead showed very strong similarities to the τ structure previously reported by van Duong et al. in an indomethacin/polyethylene glycol solid dispersion. Due to the difficulty isolating single crystals of τ for SCXRD, the structure of this polymorph remains unsolved (Van Duong *et al.*, 2018). For our structure, indexing the XRPD data was challenging, providing many possible monoclinic unit cells and space group options. Before turning to 3D-ED, several attempts to progress with structure determination from XRPD data via global optimisation methods using some of the many candidate unit cells of our structure proved unsuccessful.

The ASD was deposited as a crushed powder onto Quantifoil R1.2/1.3 grids. 3D-ED data were collected from crystals several microns in size at cryogenic conditions using a Thermo Fisher Titan Krios G3i operated at 300 kV and a CETA-16M camera, revealing a monoclinic unit cell. Based on observed systematic absences, the search was narrowed to two possible space groups: *C*2/*c* or *Cc*. While the occurrence of *Cc* structures in the CSD is rarer than *C*2/*c*, structure solution using both space groups was attempted before further conclusions were drawn.

A dataset obtained from one crystal (shown in Figure 2a) was of sufficient quality to proceed with structure solution, giving a completeness of 77% up to 0.8 Å resolution. Monoclinic cell parameters were found to be: a = 43.70(12) Å, b = 5.19(7) Å, c = 33.43 (7) Å, β = 100.73(9) °, V = 7448(104) Å^3. From the orientation matrix, the short crystallographic *b*-axis is parallel to the long axis of the crystals as might be expected from Bravais-Friedel-Donnay-Harker (Donnay & Harker, 1937) considerations. Crystals were found to lie with the (1 0 0) face flat on the grids (Figure 2a). Due to this preferred orientation of the crystals, a problem documented in 3D-ED (Lightowler *et al.*, 2022; Woollam *et al.*, 2020), it was not possible to collect to completeness of greater than 80% even with the merging of multiple crystals. Given the sufficient quality of an individual dataset, it was decided not to merge data from multiple crystals.

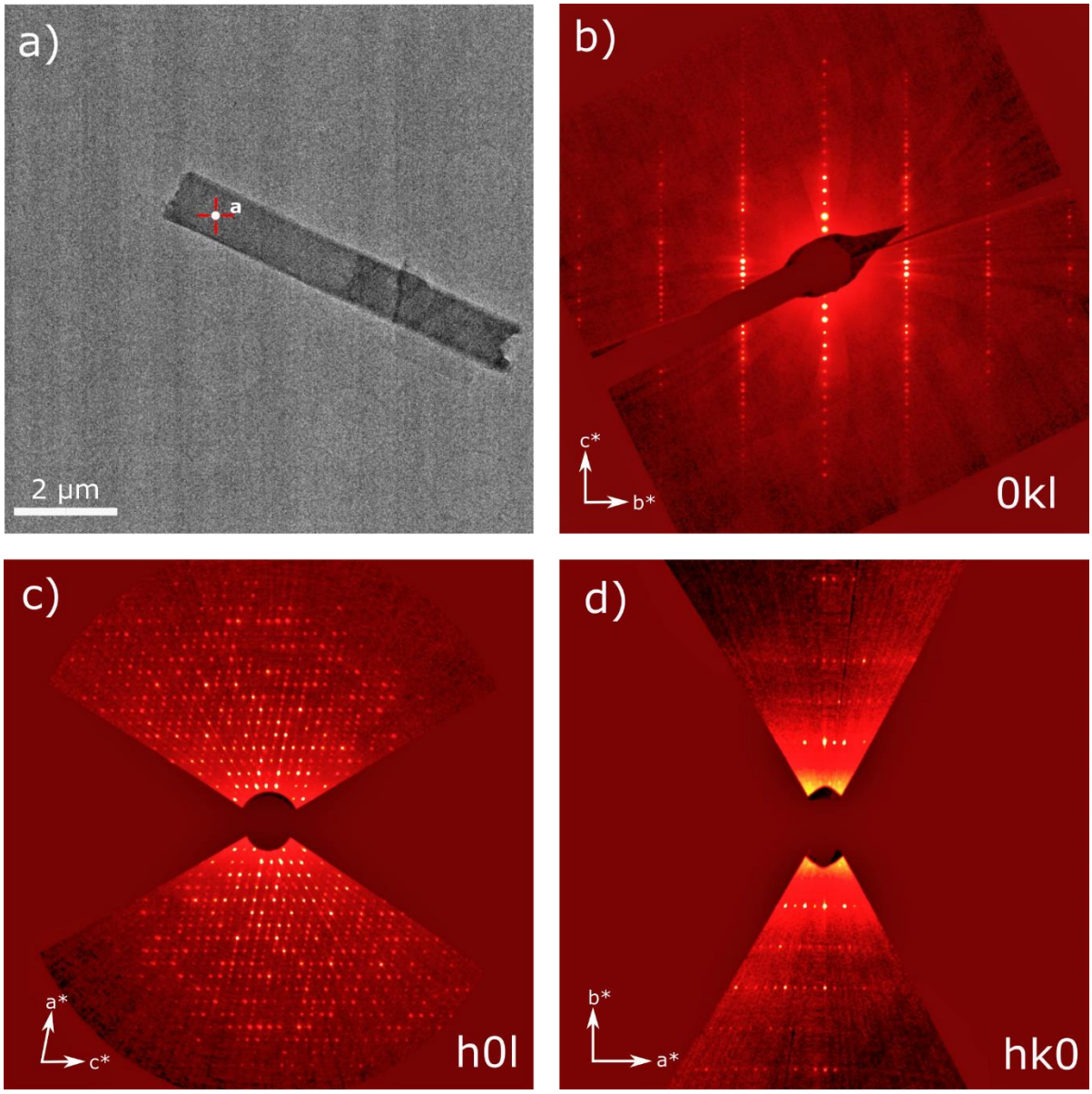

Figure 2 a) the crystal from which structure solution was successful. It is positioned such that the [1 0 0] direction is parallel to the direction of the electron beam at 0 ° tilt, based on the calculated orientation matrix. b-d) Slices of reciprocal lattice planes from reconstructed reciprocal space for indomethacin. Systematic absences suggest a monoclinic space group of *C*2/*c* or *Cc*.

3. Results and Discussion

The structure was successfully solved via the *ab initio* dual space method implemented in SHELXD (Schneider & Sheldrick, 2002) using the *C*2/*c* space group with two indomethacin molecules per asymmetric unit (*Z'* = 2). All non-hydrogen atoms were found in the initial *C*2/*c* structure solution. Hydrogen atoms were generated in geometrically idealised positions. By comparison, structure solution using the *Cc* space group only yielded a partial solution. The positions of found atoms in the incomplete C*c* solution matched the molecular conformation of those in the C2/*c* solution, but with an

origin shift. However, refinement of the partial solution was highly unstable even with restraints to control the pseudosymmetry. Therefore, final refinement was carried out using the least-squares methods in SHELXL for the *C*2/*c* space group using electron scattering factors *(International Tables Vol C: Tables 4.2.6.8 and 6.1.1.4)*. Restraints were limited to maintaining the same geometry in the two independent molecules: there was no need for any further geometric or atomic displacement restraints. Isotropic atomic displacement factors were preferred because anisotropic refinement was not found to significantly improve the model. The final model gave an *R*-factor of 28.22% refined using data to 0.8 Å resolution. Table S1 summarises all relevant crystallographic information.

Electron diffraction structures typically have higher *R*-factors than those solved using SCXRD (Klar *et al.*, 2023). In this case, this is likely due to several factors. Both structure solution and refinement have been carried out using kinematical approximations assuming intensities are proportional to the square of the structure factor ($I_{hkl} \alpha |F_{hkl}|^2$); dynamical effects (i.e. multiple scattering) which will affect the observed intensities are not considered here (Palatinus *et al.*, 2015). Another factor is the induced radiation damage to the sample. This is qualitatively described by the observation of higher order spots reducing in intensity across the tilt series. Quantitative modelling of the effects of electron beam irradiation damage are not yet well established (Peet *et al.*, 2019). The CETA camera used is also less sensitive compared to a direct electron detector and required a higher dose (a cumulative dose of 20 e $Å^{-2}$ per tilt series), thus exacerbating sample damage and accurate detection of intensities. Finally, no correction was made to account for the effects of inelastic scattering.

The asymmetric unit of the new polymorph contains two indomethacin molecules. The root mean square deviation (RMSD), a measure of the average distance between the atoms of two superimposed molecules, between the indomethacin molecules is 0.5003 Å. As can be seen in Figure 3a), the torsion angles in the carboxylic groups of the different indomethacin molecules here are orthogonal but otherwise the molecules are highly similar. By considering the overlay for all non-hydrogen atoms except the carboxylic acid oxygens, the RMSD is reduced to 0.125 Å. The independent indomethacin molecules in this polymorph form a carboxylic dimer which is consistent with interactions found in the α, γ, θ, and δ forms.

To confirm our 3D-ED model and show consistency with the bulk sample, a Rietveld rigid body refinement, starting from an idealised model of indomethacin molecular geometry with five rotatable bonds and positions obtained from 3D-ED data, was performed on XRPD synchrotron data (Figure S3). This converged with a satisfactory fit (R_{wp} = 1.40%, χ^2 = 2.09) without significant modification of the structure. Although characteristic peak positions from the new structure are very similar to that of the τ polymorph identified by van Duong et al. (Van Duong *et al.*, 2018), the relative intensities of the peaks do not match, and this cannot be accounted for by the effects of texture. Most notably, the very weak intensity of the (4 0 0) peak in the new XRPD data contrasts with the strong peak at the corresponding location in τ. This cannot be explained by preferred orientation because the lower order

peak (2 0 0) is the strongest peak detected in the new structure: this is more than 8000 times stronger than the (4 0 0), as shown in Figure S4. The difference in observed intensities in XRPD data must instead come from differences within the unit cells. It is not possible to see these peaks in electron diffraction data because these low order reflections are covered by the shadow of the beam stop, which acts to protect the electron detector from the direct beam. However, given the similar characteristic peak positions, the τ polymorph and our structure are likely closely related and share strong structural similarities. We propose to name the new structure σ, the ninth polymorph of indomethacin.

Upon further inspection of σ, we note that 12% of the unit cell volume is composed of predominantly hydrophobic open channels parallel to the *b*-axis (Figure 3c). Large void spaces in crystal structures can be associated with metastable phases (Kitaigorodskii, 1965; Barbas et al., 2018; Sundareswaran & Karuppannan, 2020). The metastable nature of polymorph σ relative to the most thermodynamically stable γ phase is supported by the emergence of new peaks corresponding to the latter phase in XRPD data collected around 10 months after the production of σ. Based on the spatial distribution of the channels, we considered the possibility that a smaller molecule (such as solvent) is responsible for the empty space in the structure and relevant to the crystallisation mechanism of σ. We propose that dichloromethane molecules (the solvent used) may have acted as a backbone solvent template, running in channels through the structure during solvent evaporation as crystals formed. The total channel volume in the unit cell is 903 $Å^3$, with 8 channels in each unit cell. The molar volume of dichloromethane is ~ 68 $Å^3$, suggesting that each channel could fit two solvent molecules given that we would expect channels in the structure to decrease in volume upon desolvation. Dichloromethane's volatility makes it highly unlikely to remain within the indomethacin structure on drying. This is further reinforced by the lack of residual electron density observed in the channels. To confirm this hypothesis, evaporation of a dichloromethane solution of pure indomethacin was carried out (on a crystallisation dish left at room temperature, with no additional heating or pressure necessary), also yielding the σ structure observed using XRPD. This is consistent with the theory of crystallisation via solvent templating (Gnutzmann *et al.*, 2014; Klimakow *et al.*, 2010).

Consequently, based on our observations from the solved structure, we have developed a simpler route to forming this polymorph. Although dichloromethane is not a solvent generally used in manufacturing processes within the pharmaceutical industry due to its environmental impact, the more open structure of this metastable form of indomethacin may be of potential interest as it will likely have different dissolution properties compared to the most thermodynamically stable γ phase. A similar theory was proposed for the crystallisation of the δ polymorph whereby the indomethacin methanol solvate first crystallises before desolvation (Andrusenko *et al.*, 2021). However, the methanol directly disrupts the hydrogen bonding between indomethacin molecules whereas in σ, the positions of the channels suggest that the dichloromethane molecules do not interact strongly with

indomethacin, as would be expected based on its lack of hydrogen bond donors and acceptors. Interestingly, although σ and δ have different packing arrangements, the conformations of the individual indomethacin molecules are broadly comparable (an example of this conformational fit is shown in Figure 3b).

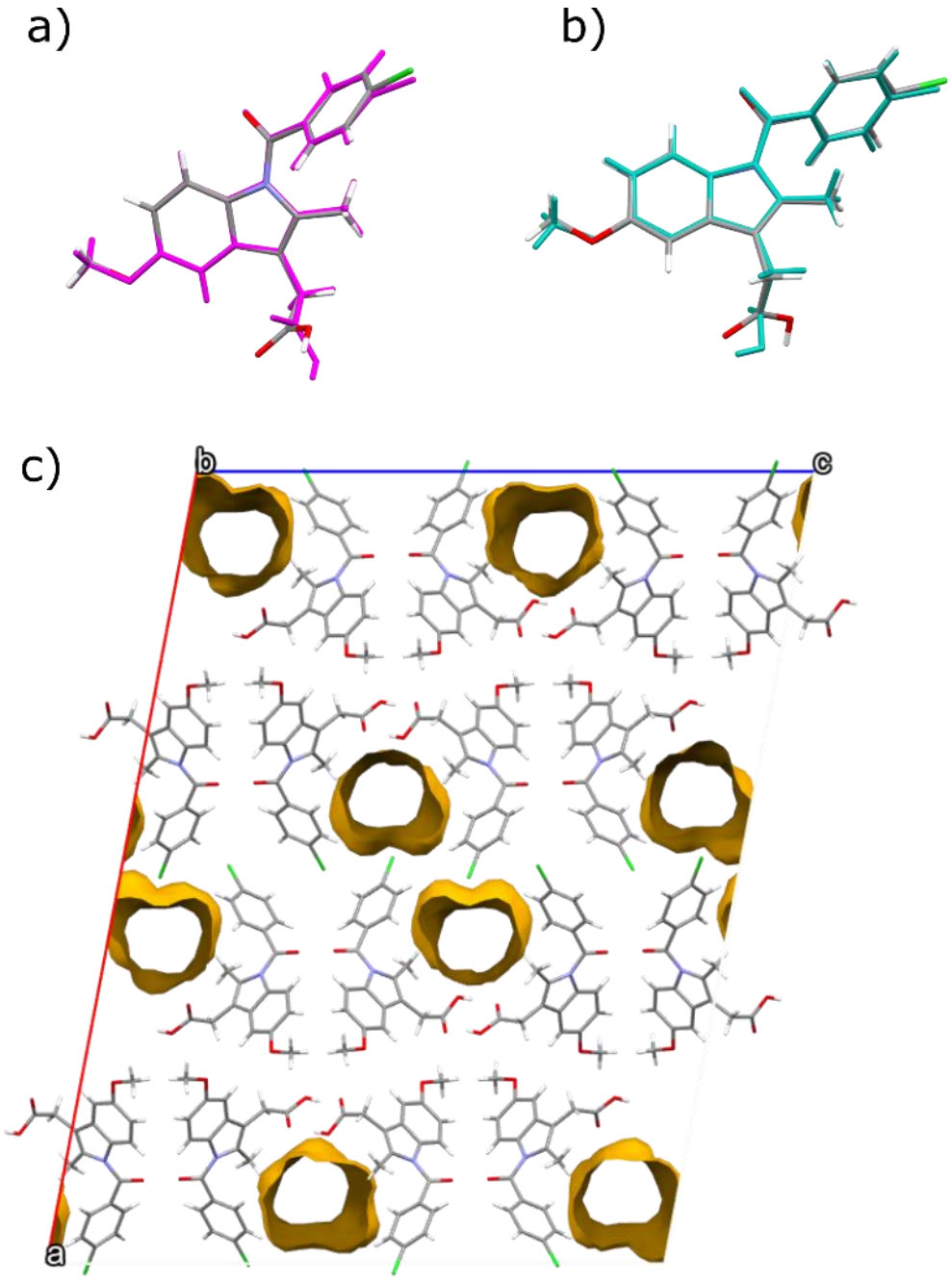

Figure 3 a) comparison between the two independent molecules of σ shows their conformational similarity. (RMSD = 0.5003 Å). The biggest difference comes from the torsion angle of the carboxylic groups. Overlaying all atoms except the carboxylic acid oxygens leads to RMSD = 0.125 Å. b) a conformational comparison between one of the indomethacin molecules in σ with one of the independent molecules in the δ structure (RMSD = 0.392 Å). Similarly to (a), the difference comes

from the torsion angle of the carboxylic groups. Overlaying all atoms except the carboxylic acid oxygens leads to RMSD = 0.153 Å. c) Yellow graphics highlight the channels in the σ structure which suggests that solvent templating was the mechanism for formation.

In conclusion, we have isolated a metastable phase of indomethacin from an amorphous solid dispersion and reported the structure of a new polymorph (which we call σ) using 3D-ED. The solution obtained suggested a crystallisation mechanism of solvent templating and provided an easier experimental route to the new form via evaporation of pure indomethacin from dichloromethane. This demonstrates the applicability of 3D-ED to drug development in addition to drug discovery.

Acknowledgements We thank Rigaku for access to the CrysAlisPro software suite.

Funding Information HL and PAM acknowledge funding from grants EPSRC (EP/R00879/1) and a GSK ICASE (210193) studentship. We also thank Diamond Light Source for access and support in use of the I11 beam (proposal number CY34800) that contributed to the results presented here.

References

Andrusenko, I., Hamilton, V., Lanza, A. E., Hall, C. L., Mugnaioli, E., Potticary, J., Buanz, A., Gaisford, S., Piras, A. M., Zambito, Y., Hall, S. R. & Gemmi, M. (2021). *Int. J. Pharm.* **608**, 121067.

Barbas, R., Font-Bardia, M. & Prohens, R. (2018). *Cryst. Growth Des.* **18**, 3740–3746.

Butler, J. M. & Dressman, J. B. (2010). *J. Pharm. Sci.* **99**, 4940–4954.

Chen, X., Morris, K. R., Griesser, U. J., Byrn, S. R. & Stowell, J. G. (2002). *J. Am. Chem. Soc.* **124**, 15012–15019.

Coelho, A. A. (2018). *J. Appl. Crystallogr.* **51**, 210–218.

Donnay, J. D. H. & Harker, D. (1937). *Am. Mineral.* **22**, 446–467.

Van Duong, T., Lüdeker, D., Van Bockstal, P. J., De Beer, T., Van Humbeeck, J. & Van Den Mooter, G. (2018). *Mol. Pharm.* **15**, 1037–1051.

Gemmi, M., Mugnaioli, E., Gorelik, T. E., Kolb, U., Palatinus, L., Boullay, P., Hovmö, S. & Abrahams, J. P. (2019). *ACS Cent. Sci.* **5**, 1315–1329.

Gnutzmann, T., Nguyen Thi, Y., Rademann, K. & Emmerling, F. (2014). *Cryst. Growth Des.* **14**, 6445–6450.

Gruene, T., Wennmacher, J. T. C., Zaubitzer, C., Holstein, J. J., Heidler, J., Fecteau-Lefebvre, A., De Carlo, S., Müller, E., Goldie, K. N., Regeni, I., Li, T., Santiso-Quinones, G., Steinfeld, G., Handschin, S., van Genderen, E., van Bokhoven, J. A., Clever, G. H. & Pantelic, R. (2018).

Angew. Chemie - Int. Ed. **57**, 16313–16317.

Guzmán, H. R., Tawa, M., Zhang, Z., Ratanabanangkoon, P., Shaw, P., Gardner, C. R., Chen, H., Moreau, J. P., Almarsson, Ö. & Remenar, J. F. (2007). *J. Pharm. Sci.* **96**, 2686–2702.

He, Y. & Ho, C. (2015). *J. Pharm. Sci.* **104**, 3237–3258.

Hu, C., Hu, C., Liu, Z., Liu, C., Li, J., Wang, Z., Xu, L., Chen, C., Fan, H. & Qian, F. (2019). *Mol. Pharm.* **16**, 4978–4986.

Jones, C. G., Martynowycz, M. W., Hattne, J., Fulton, T. J., Stoltz, B. M., Rodriguez, J. A., Nelson, H. M. & Gonen, T. (2018). *ACS Cent. Sci.* **4**, 1587–1592.

Karothu, D. P., Alhaddad, Z., Göb, C. R., Schürmann, C. J., Bücker, R. & Naumov, P. (2023). *Angew. Chemie Int. Ed.* **62**, e202303761.

Kistenmacher, T. J. & Marsh, R. E. (1972). *J. Am. Chem. Soc.* **94**, 1340–1345.

Kitaigorodskii, A. I. (1965). *Acta Crystallogr.* **18**, 585–590.

Klar, P. B., Krysiak, Y., Xu, H., Steciuk, G., Cho, J., Zou, X. & Palatinus, L. (2023). *Nat. Chem. 2023 156* **15**, 848–855.

Klimakow, M., Leiterer, J., Kneipp, J., Rössler, E., Panne, U., Rademann, K. & Emmerling, F. (2010). *Langmuir* **26**, 11233–11237.

Lightowler, M., Li, S., Ou, X., Cho, J., Liu, B., Li, A., Hofer, G., Xu, J., Yang, T., Zou, X., Lu, M. & Xu, H. (2024). *Angew. Chemie Int. Ed.* **63**, e202317695.

Lightowler, M., Li, S., Ou, X., Zou, X., Lu, M. & Xu, H. (2022). *Angew. Chemie Int. Ed.* **61**, e202114985.

MacRae, C. F., Sovago, I., Cottrell, S. J., Galek, P. T. A., McCabe, P., Pidcock, E., Platings, M., Shields, G. P., Stevens, J. S., Towler, M. & Wood, P. A. (2020). *J. Appl. Crystallogr.* **53**, 226–235.

Newman, A. & Wenslow, R. (2016). *AAPS Open 2016 21* **2**, 1–11.

Palatinus, L., Corrêa, C. A., Steciuk, G., Jacob, D., Roussel, P., Boullay, P., Klementová, M., Gemmi, M., Kopeček, J., Domeneghetti, M. C., Cámara, F. & Petříček, V. (2015). *Acta Crystallogr. Sect. B Struct. Sci. Cryst. Eng. Mater.* **71**, 740–751.

Peet, M. J., Henderson, R. & Russo, C. J. (2019). *Ultramicroscopy* **203**, 125–131.

Pham, T. N., Watson, S. A., Edwards, A. J., Chavda, M., Clawson, J. S., Strohmeier, M. & Vogt, F. G. (2010). *Mol. Pharm.* **7**, 1667–1691.

Ricarte, R. G., Van Zee, N. J., Li, Z., Johnson, L. M., Lodge, T. P. & Hillmyer, M. A. (2019). *Mol.*

Pharm. **16**, 4089–4103.

Rigaku Oxford Diffraction (2020).

S'ari, M., Blade, H., Cosgrove, S., Drummond-Brydson, R., Hondow, N., Hughes, L. P. & Brown, A. (2021). *Mol. Pharm.* **18**, 1905–1919.

Schneider, T. R. & Sheldrick, G. M. (2002). *Acta Cryst D* **58**, 1772–1779.

Sundareswaran, S. & Karuppannan, S. (2020). *Cryst. Res. Technol.* **55**, 2000083.

Surwase, S. A., Boetker, J. P., Saville, D., Boyd, B. J., Gordon, K. C., Peltonen, L. & Strachan, C. J. (2013). *Mol. Pharm.* **10**, 4472–4480.

Vasconcelos, T., Sarmento, B. & Costa, P. (2007). *Drug Discov. Today* **12**, 1068–1075.

Woollam, G. R., Das, P. P., Mugnaioli, E., Andrusenko, I., Galanis, A. S., Van De Streek, J., Nicolopoulos, S., Gemmi, M. & Wagner, T. (2020). *CrystEngComm* **22**, 7490–7499.

Xie, T. & Taylor, L. S. (2017). *J. Pharm. Sci.* **106**, 100–110.

Supporting information

S1. Experimental Procedures

S1.1. Solvent Evaporation

Amorphous solid dispersions (ASDs) of indomethacin and polyvinylpyrrolidone (PVP) were prepared using the solvent evaporation method as described by Pham et al. (Pham *et al.*, 2010). Indomethacin and PVP K25, purchased from Sigma Aldrich, were weighed to make up a combined mass of 0.5 g. ASDs with a range of drug loadings from 20:80 wt% to 95:5 wt% indomethacin/PVP were made. The powder was dissolved in approximately 10 cm^3 of dicholoromethane to form a yellow solution. A rotary evaporator was used to boil off the dichloromethane solvent which was placed in a water bath at 40 °C under a pressure of 40 mBar. The resulting powder coated the glass vial which was then placed in a vacuum overnight to ensure any remaining solvent was evaporated. Prior to use, each sample was stored at room temperature in a dessicator.

S1.2. X-Ray Powder Diffraction

In-situ XRPD characterisation was performed at Diamond beamline I11. ASD powder was loaded into a 0.5 mm borosilicate glass capillary and analysed using an X-ray beam of 0.82408 Å wavelength (15 keV energy), refined using a NIST SRM640c Si standard. The sample was cooled to 80 K, consistent with 3D-ED measurement conditions, using a Cryostream Plus. Measurements were made using the Mythen wide-angle position sensitive detector (PSD).

S1.3. 3D-ED sample preparation and data collection

3D-ED was performed under cryogenic conditions using a Thermo Fisher Titan Krios G3i operated at 300 kV and a CETA-16M camera. A diffraction pattern was recorded for each tilt increment over a range of ± 60 ° where the relative position of the crystal of interest with respect to the grid bars or other crystals would allow at a continuous tilt rate of 1 °/s, with an exposure time of 0.5 s per frame, leading to 240 frames. EPU-D software was used for this acquisition, and the auto-eucentric height function was used to minimise sample movement when tilting to high angles. Despite this correction, 3D-ED could only be performed on the larger lath-like crystals due to the significant relative image movement of the whisker-like crystals.

3D-ED data were recorded from 10 different crystals with sizes ranging between 100 nm to several microns. EPU-D software was used to capture information relating to crystal morphologies in low magnification mode on the TEM to easily direct us to crystals that were ideally positioned and isolated. Camera lengths were set such that the edge of the detector allowed for a resolution of 0.75 Å. Well-isolated crystals which displayed little evidence of significant mosaicity (as observed in diffraction mode) gave clean diffraction patterns and were selected for further data analysis.

S2. Results and Discussion

S2.1. 3D-ED Data Processing

3D-ED data were analysed using Rigaku CrysAlisPro 1.171.41.93a) software (Rigaku Oxford Diffraction, 2020), which allowed for reciprocal space reconstruction and visualisation, cell parameter determination, and reflection intensity integration. This analysis revealed consistent symmetry and lattice constants between different crystals. Out of 10 datasets deemed high enough quality for further analysis, reciprocal reconstruction revealed one of these crystals was the (already solved) α phase. The rest were consistent with the monoclinic unit cell of the σ polymorph and were used to confirm unit cell parameters.

The best dataset was used for structure determination and refinement with the *C*2/*c* space group. The Olex2 interface was used to access SHELXD and SHELXL for structure solution and refinement respectively. Refined structures were subsequently analysed using Mercury software (MacRae *et al.*, 2020), taking advantage of its tools for conformational comparison between molecules and void calculation.

S2.2. Rietveld Refinement from X-Ray Powder Diffraction

With a crystal structure of σ indomethacin having been obtained from 3D-ED methods, we returned to XRPD to ensure the validity of the structure by carrying out refinement using the 3D-ED model. Rietveld refinement was carried out using TOPAS academic software (Coelho, 2018). The measurement of an empty capillary was used as an empirical background with a scale factor which was set as a refinable parameter. On top of this, the background was further described with a 6-parameter Chebyshev function. Pawley fitting showed significant anisotropy which was modelled with spherical harmonics and strain. The indomethacin molecule was modelled as a rigid body with the same positions and orientations as in the σ molecules where the torsion angles associated with the five rotatable bonds were freely refined based on its idealised initial geometry from the γ structure solved by SCXRD (CCDC ref 1180373). The refinement converged to R_{wp} = 1.40% and χ^2 = 2.09.

S3. Supporting Tables

Empirical formula	C_{19} H_{16} Cl N O_4	
Formula weight	357.79	
Temperature	87(2) K	
Wavelength	0.0197 Å	
Crystal system	Monoclinic	
Space group	C 2/c	
Unit cell dimensions	a = 43.70(12) Å	α= 90°.
	b = 5.19(7) Å	β= 100.73(9)°.
	c = 33.43(7) Å	γ = 90°.
Volume	7448(104) $Å^3$	
Z	16	
Density (calculated)	1.276 Mg/m^3	
Absorption coefficient	0.000 mm^{-1}	
F(000)	1114*	
Crystal size	0.0070 x 0.0010 x 0.0001 mm^3	
Theta range for data collection	0.057 to 0.705°.	
Index ranges	-48<=h<=47, -6<=k<=6, -41<=l<=41	
Reflections collected	15410	
Independent reflections	5885 [R(int) = 0.1371]	
Absorption correction	Semi-empirical from equivalents	
Max. and min. transmission	1.00000 and 0.01541	
Refinement method	Full-matrix least-squares on F^2	
Data / restraints / parameters	5885 / 66 / 208	
Goodness-of-fit on F^2	1.165	
Final R indices [I>2sigma(I)]	R1 = 0.2822, wR2 = 0.6107	
R indices (all data)	R1 = 0.3254, wR2 = 0.6347	
Extinction coefficient	534(71)	
Largest diff. peak and hole	0.452 and -0.423 e.$Å^{-3}$	

Table S1 Selected parameters from the structure refinement using SHELXL, generated by XCIF. The structure solution and refinement executed here makes use of workflows which come from X-ray crystallography protocols. As such, we recognise that some parameters are not ideal for use with electron diffraction. For example, the semi-empirical absorption corrections here likely account for

effects of beam damage whilst small Bragg angles associated with electron diffraction data likely contribute to larger EXTI parameters (and larger errors in this value). However, refinement without these semi-empirical corrections led to a worse model and higher R-factor. *Number of electrons in the unit cell.

S4. Supporting Figures

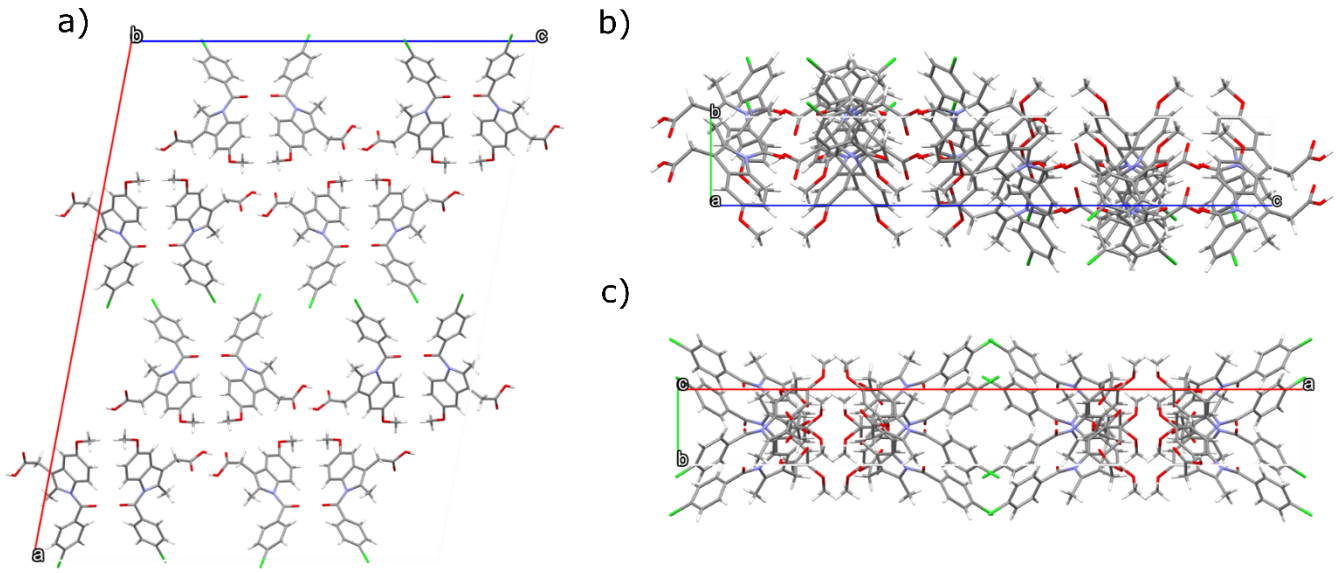

Figure S1 Molecular packing of the σ indomethacin structure viewed along a) *b*-axis, b) *a*-axis, c) *c*-axis.

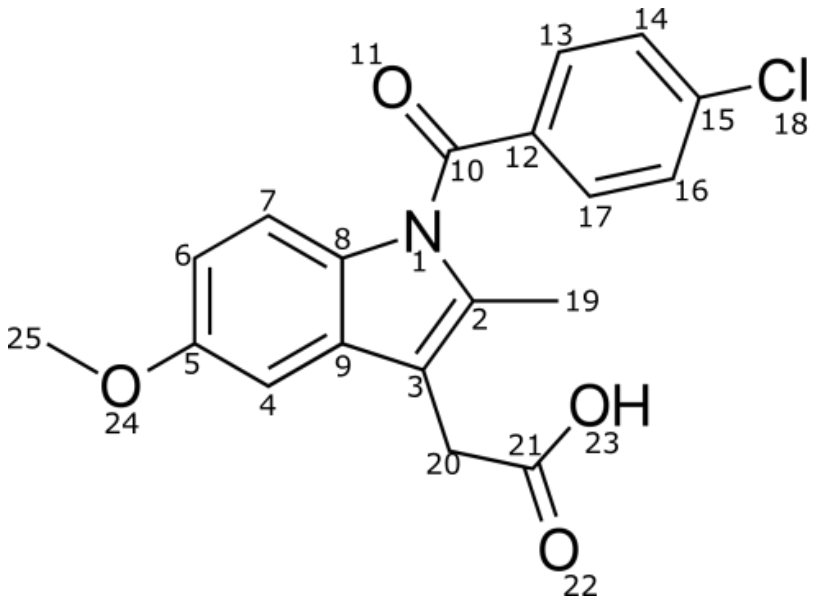

Figure S2 Labels used for structure refinement of indomethacin. The 2nd indomethacin molecule in the asymmetric unit has identical labels, except starting from N50 (50 is added to all numbers).

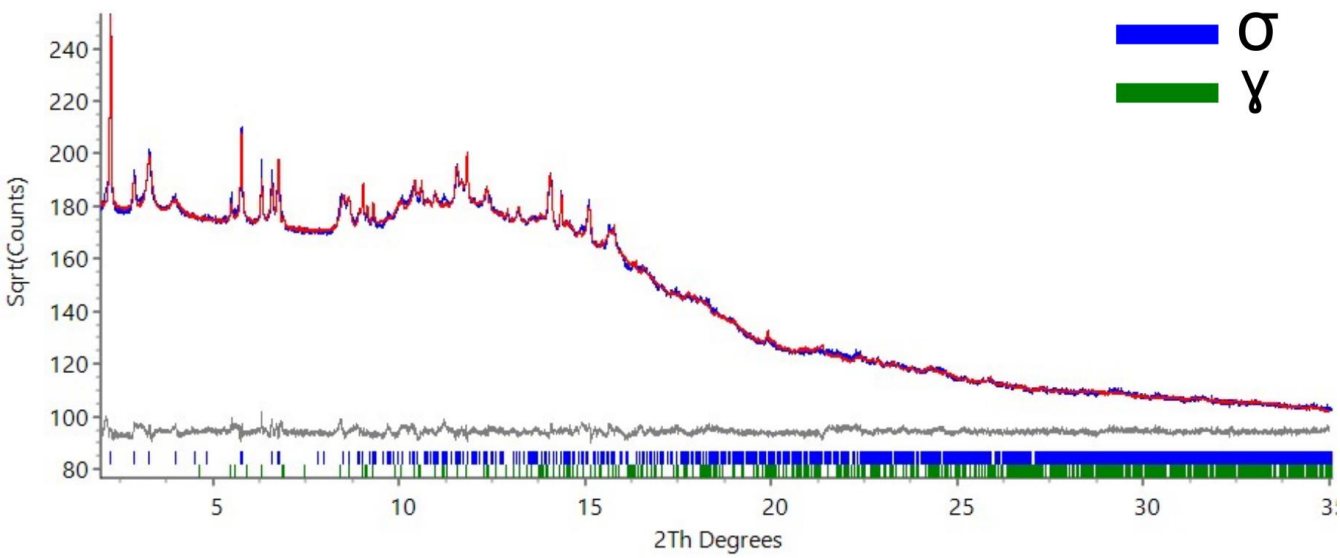

Figure S3 Rietveld Refinement of high resolution XRPD data using the structural model obtained from 3D-ED. This shows consistency between the bulk powder and single crystal data. R_{wp} = 1.40% and χ^2 = 2.09. The presence of the γ phase is also modelled in this refinement.

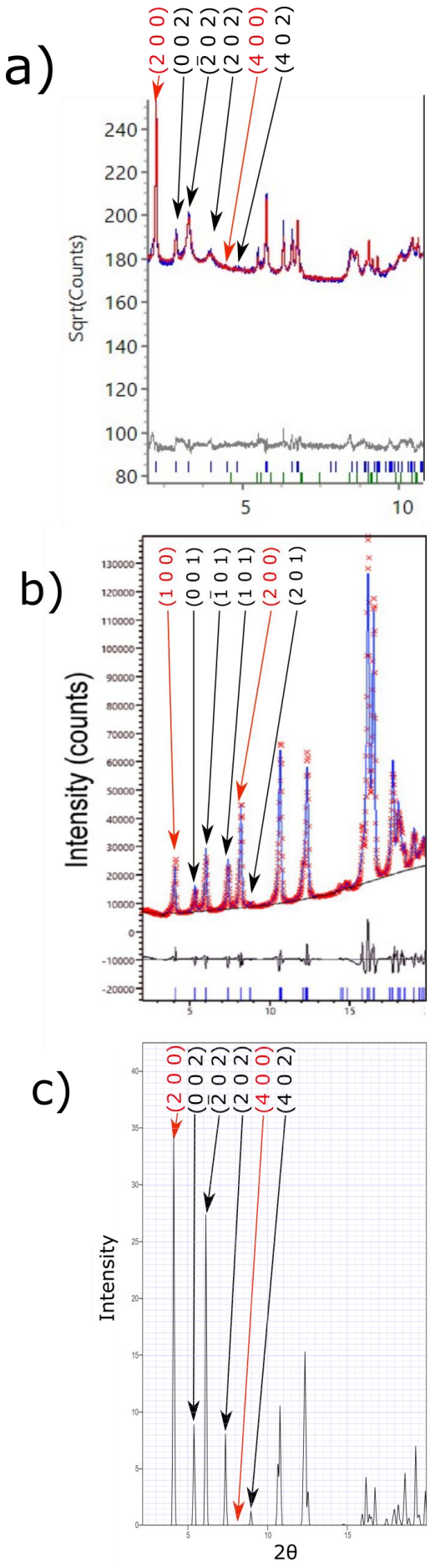
a)
(2 0 0)
(0 0 2)
(2̄ 0 2)
(2 0 2)
(4 0 0)
(4 0 2)
Sqrt(Counts)
b)
(1 0 0)
(0 0 1)
(1̄ 0 1)
(1 0 1)
(2 0 0)
(2 0 1)
Intensity (counts)
c)
(2 0 0)
(0 0 2)
(2̄ 0 2)
(2 0 2)
(4 0 0)
(4 0 2)
Intensity
2θ

Figure S4 A comparison of the XRPD trace from (a) our σ structure (λ = 0.82408 Å), (b) the unsolved τ structure (λ = 1.54060 Å) (Van Duong *et al.*, 2018), and (c) our σ structure (simulated at λ = 1.54060 Å for easier comparison as the differences in wavelength used for experiments means the experimental peak positions cannot be directly overlaid). Furthermore, a different proposed unit cell leads to different indexing of the resulting peaks. However, we point to the differences in relative intensities in (a) and (c) between the $(2\ 0\ 0)_\sigma$, the strongest peak, and $(4\ 0\ 0)_\sigma$, a peak almost absent in our structure compared to in (b) the corresponding $(1\ 0\ 0)_\tau$ and $(2\ 0\ 0)_\tau$ peaks, where the $(2\ 0\ 0)_\tau$ peak in τ is even stronger than $(1\ 0\ 0)_\tau$. This cannot be explained by effects of texture because related parallel crystal planes (e.g. $(2\ 0\ 0)_\sigma$, $(4\ 0\ 0)_\sigma$ and $(1\ 0\ 0)_\tau$, $(2\ 0\ 0)_\tau$ should be affected in the same way by preferred orientation. *(b) Reprinted (adapted) with permission from {Tu Van Duong et al., Molecular Pharmaceutics 2018 15 (3), 1037-105, 10.1021/acs.molpharmaceut.7b00930}. Copyright {2018} American Chemical Society.*

References

Andrusenko, I., Hamilton, V., Lanza, A. E., Hall, C. L., Mugnaioli, E., Potticary, J., Buanz, A., Gaisford, S., Piras, A. M., Zambito, Y., Hall, S. R. & Gemmi, M. (2021). *Int. J. Pharm.* **608**, 121067.

Barbas, R., Font-Bardia, M. & Prohens, R. (2018). *Cryst. Growth Des.* **18**, 3740–3746.

Butler, J. M. & Dressman, J. B. (2010). *J. Pharm. Sci.* **99**, 4940–4954.

Chen, X., Morris, K. R., Griesser, U. J., Byrn, S. R. & Stowell, J. G. (2002). *J. Am. Chem. Soc.* **124**, 15012–15019.

Coelho, A. A. (2018). *J. Appl. Crystallogr.* **51**, 210–218.

Donnay, J. D. H. & Harker, D. (1937). *Am. Mineral.* **22**, 446–467.

Van Duong, T., Lüdeker, D., Van Bockstal, P. J., De Beer, T., Van Humbeeck, J. & Van Den Mooter, G. (2018). *Mol. Pharm.* **15**, 1037–1051.

Gemmi, M., Mugnaioli, E., Gorelik, T. E., Kolb, U., Palatinus, L., Boullay, P., Hovmö, S. & Abrahams, J. P. (2019). *ACS Cent. Sci.* **5**, 1315–1329.

Gnutzmann, T., Nguyen Thi, Y., Rademann, K. & Emmerling, F. (2014). *Cryst. Growth Des.* **14**, 6445–6450.

Gruene, T., Wennmacher, J. T. C., Zaubitzer, C., Holstein, J. J., Heidler, J., Fecteau-Lefebvre, A., De Carlo, S., Müller, E., Goldie, K. N., Regeni, I., Li, T., Santiso-Quinones, G., Steinfeld, G.,

Handschin, S., van Genderen, E., van Bokhoven, J. A., Clever, G. H. & Pantelic, R. (2018). *Angew. Chemie - Int. Ed.* **57**, 16313–16317.

Guzmán, H. R., Tawa, M., Zhang, Z., Ratanabanangkoon, P., Shaw, P., Gardner, C. R., Chen, H., Moreau, J. P., Almarsson, Ö. & Remenar, J. F. (2007). *J. Pharm. Sci.* **96**, 2686–2702.

He, Y. & Ho, C. (2015). *J. Pharm. Sci.* **104**, 3237–3258.

Hu, C., Hu, C., Liu, Z., Liu, C., Li, J., Wang, Z., Xu, L., Chen, C., Fan, H. & Qian, F. (2019). *Mol. Pharm.* **16**, 4978–4986.

Jones, C. G., Martynowycz, M. W., Hattne, J., Fulton, T. J., Stoltz, B. M., Rodriguez, J. A., Nelson, H. M. & Gonen, T. (2018). *ACS Cent. Sci.* **4**, 1587–1592.

Karothu, D. P., Alhaddad, Z., Göb, C. R., Schürmann, C. J., Bücker, R. & Naumov, P. (2023). *Angew. Chemie Int. Ed.* **62**, e202303761.

Kistenmacher, T. J. & Marsh, R. E. (1972). *J. Am. Chem. Soc.* **94**, 1340–1345.

Kitaigorodskii, A. I. (1965). *Acta Crystallogr.* **18**, 585–590.

Klar, P. B., Krysiak, Y., Xu, H., Steciuk, G., Cho, J., Zou, X. & Palatinus, L. (2023). *Nat. Chem. 2023 156* **15**, 848–855.

Klimakow, M., Leiterer, J., Kneipp, J., Rössler, E., Panne, U., Rademann, K. & Emmerling, F. (2010). *Langmuir* **26**, 11233–11237.

Lightowler, M., Li, S., Ou, X., Cho, J., Liu, B., Li, A., Hofer, G., Xu, J., Yang, T., Zou, X., Lu, M. & Xu, H. (2024). *Angew. Chemie Int. Ed.* **63**, e202317695.

Lightowler, M., Li, S., Ou, X., Zou, X., Lu, M. & Xu, H. (2022). *Angew. Chemie Int. Ed.* **61**, e202114985.

MacRae, C. F., Sovago, I., Cottrell, S. J., Galek, P. T. A., McCabe, P., Pidcock, E., Platings, M., Shields, G. P., Stevens, J. S., Towler, M. & Wood, P. A. (2020). *J. Appl. Crystallogr.* **53**, 226–235.

Newman, A. & Wenslow, R. (2016). *AAPS Open 2016 21* **2**, 1–11.

Palatinus, L., Corrêa, C. A., Steciuk, G., Jacob, D., Roussel, P., Boullay, P., Klementová, M., Gemmi, M., Kopeček, J., Domeneghetti, M. C., Cámara, F. & Petříček, V. (2015). *Acta Crystallogr. Sect. B Struct. Sci. Cryst. Eng. Mater.* **71**, 740–751.

Peet, M. J., Henderson, R. & Russo, C. J. (2019). *Ultramicroscopy* **203**, 125–131.

Pham, T. N., Watson, S. A., Edwards, A. J., Chavda, M., Clawson, J. S., Strohmeier, M. & Vogt, F. G. (2010). *Mol. Pharm.* **7**, 1667–1691.

Ricarte, R. G., Van Zee, N. J., Li, Z., Johnson, L. M., Lodge, T. P. & Hillmyer, M. A. (2019). *Mol. Pharm.* **16**, 4089–4103.

Rigaku Oxford Diffraction (2020).

S'ari, M., Blade, H., Cosgrove, S., Drummond-Brydson, R., Hondow, N., Hughes, L. P. & Brown, A. (2021). *Mol. Pharm.* **18**, 1905–1919.

Schneider, T. R. & Sheldrick, G. M. (2002). *Acta Cryst D* **58**, 1772–1779.

Sundareswaran, S. & Karuppannan, S. (2020). *Cryst. Res. Technol.* **55**, 2000083.

Surwase, S. A., Boetker, J. P., Saville, D., Boyd, B. J., Gordon, K. C., Peltonen, L. & Strachan, C. J. (2013). *Mol. Pharm.* **10**, 4472–4480.

Vasconcelos, T., Sarmento, B. & Costa, P. (2007). *Drug Discov. Today* **12**, 1068–1075.

Woollam, G. R., Das, P. P., Mugnaioli, E., Andrusenko, I., Galanis, A. S., Van De Streek, J., Nicolopoulos, S., Gemmi, M. & Wagner, T. (2020). *CrystEngComm* **22**, 7490–7499.

Xie, T. & Taylor, L. S. (2017). *J. Pharm. Sci.* **106**, 100–110.